


Noncollinear Spin Current for Switching of Chiral Magnetic Textures

Dongwook Go^{1,2,*}, Moritz Sallermann^{1,3}, Fabian R. Lux², Stefan Blügel¹,
Olena Gomonay² and Yuriy Mokrousov^{1,2,†}

¹*Peter Grünberg Institut and Institute for Advanced Simulation, Forschungszentrum Jülich and JARA, 52425 Jülich, Germany*

²*Institute of Physics, Johannes Gutenberg University Mainz, 55099 Mainz, Germany*

³*Science Institute and Faculty of Physical Sciences, University of Iceland, VR-III, 107 Reykjavík, Iceland*

 (Received 23 February 2022; revised 10 June 2022; accepted 25 July 2022; published 26 August 2022)

We propose a concept of noncollinear spin current, whose spin polarization varies in space even in nonmagnetic crystals. While it is commonly assumed that the spin polarization of the spin Hall current is uniform, asymmetric local crystal potential generally allows the spin polarization to be noncollinear in space. Based on microscopic considerations, we demonstrate that such noncollinear spin Hall currents can be observed, for example, in layered Kagome Mn_3X ($X = Ge, Sn$) compounds. Moreover, by referring to atomistic spin dynamics simulations we show that noncollinear spin currents can be used to switch the chiral spin texture of Mn_3X in a deterministic way even in the absence of an external magnetic field. Our theoretical prediction can be readily tested in experiments, which will open a novel route toward electric control of complex spin structures in noncollinear antiferromagnets.

DOI: [10.1103/PhysRevLett.129.097204](https://doi.org/10.1103/PhysRevLett.129.097204)

Recent studies have shown that antiferromagnets (AFMs) can take the role of ferromagnets in spintronics [1,2] for their promising features such as the high frequency nature of eigenmodes, which offers a unique opportunity to study ultrafast dynamics at terahertz frequencies [3–5]. Furthermore, the resilience to an external magnetic field and absence of stray fields make AFMs advantageous for increasing the memory density. However, these properties make manipulating magnetic order in AFMs extremely difficult. One of the major breakthroughs to an era of antiferromagnetic spintronics was a realization that magnetic moments in an AFM can be electrically controlled at an atomic scale due to “locally” asymmetric environment within each sublattice, even when the global inversion symmetry is present [6–8]. While early studies have focused on collinear AFMs such as $CuMnAs$ [7] and Mn_2Au [9–11], in recent years, frustrated noncollinear (NC) AFMs such as Mn_3X ($X = Sn, Ge$) and Mn_3Ir attracted a great deal of attention. Despite a vanishingly small net magnetic moment, they exhibit pronounced anomalous Hall effect [12–15], anomalous Nernst effect [16,17], and magneto-optical Kerr effect [18], which is in clear contrast to a common wisdom of conventional ferromagnets. These effects are driven by momentum-space Berry curvature originating from the chiral spin texture in real space [12,19]. In particular, Mn_3Sn is identified as a magnetic Weyl semimetal [19], which exhibits magneto-transport phenomena of topological origin, e.g., chiral anomaly [20,21]. Here, change of the magnetic structure subsequently affects topology of the band structure, which provides an exciting platform to study an interplay of chiral magnetic texture and electron band topology [22].

However, complexity of magnetic interactions and excitations makes manipulation of the magnetic moments in NC AFMs even more challenging than in collinear AFMs. Nonetheless, Tsai *et al.* succeeded in switching the magnetic state in polycrystalline Mn_3Sn/Pt heterostructures by using the spin Hall effect (SHE) of Pt under an external magnetic field [22]. Meanwhile, Takeuchi *et al.* investigated epitaxial Mn_3Sn/Pt heterostructures and discovered a coherent rotation of the chiral spin texture in the Kagome plane [23], as predicted by Refs. [24,25]. However, we note that Refs. [22,23] used a conventional spin Hall current to induce magnetic excitations in Mn_3Sn , which to some extent is analogous to a situation in heavy metal-ferromagnet bilayers.

A unique feature of AFMs is the sublattice degree of freedom, which allows for multiple modes of excitations. Keeping this in mind, we explore the possibility of a sublattice-dependent generation of spin Hall currents and investigate how they affect the dynamics of the magnetic texture in NC AFMs. While it is well-known that the spin polarization of the spin Hall current is orthogonal to both an external electric field and current propagation direction in cubic crystals without a sublattice degree of freedom [26] [Fig. 1(a)], we find by symmetry arguments that the spin polarization of the spin Hall current can be NC in space already at the level of a nonmagnetic crystal [Fig. 1(b)]. We demonstrate that such NC spin current can be generated in Mn_3X compounds, and it exhibits a “chiral” component, which can be used to ignite a sublattice-dependent magnetization dynamics resulting in a switching of the magnetic texture. We believe that exploring the physics of sublattice-dependent NC spin currents would enrich our

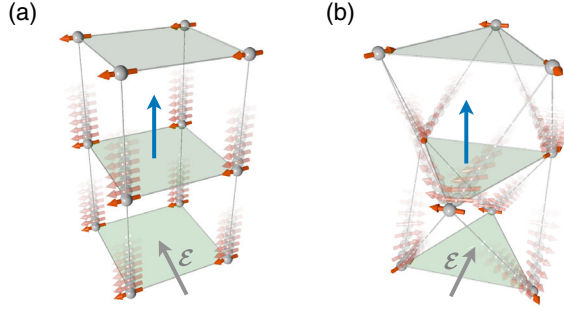


FIG. 1. Schematic illustration of the (a) conventional versus (b) NC spin Hall currents. The red arrows represent the direction of the spin polarization, the blue arrows indicate the electron's propagation direction in average, and the gray arrows represent the direction of an external electric field \mathcal{E} .

understanding of dynamics and excitations in various magnetic materials, and might provide a new way of efficient electric control of magnetic order.

First, we generalize the concept of a spin current to describe “local” components in the vicinity of individual atoms, whose polarization may differ depending on the sublattice. The local spin current on site i can be defined from the “global” spin current $\mathbf{Q} = \mathbf{v} \otimes \mathbf{S}$ by $\mathbf{Q}_i = (\mathbf{Q}P_i + P_i\mathbf{Q})/2$, where \mathbf{v} is the velocity operator, \mathbf{S} is the spin operator, and P_i is the projection operator on site i , such that $\mathbf{Q} = \sum_i \mathbf{Q}_i$ [27]. Given an external electric field \mathcal{E} , the local spin Hall conductivity (SHC) tensor on site i , $\sigma_{\alpha\beta}^{S_\gamma}$ is defined by $Q_{\alpha\beta,i} = \sigma_{\alpha\gamma,i}^{S_\beta} \mathcal{E}_\gamma$, where α, β, γ stand for Cartesian components of the velocity, spin, and external electric field, respectively. The global SHC is recovered by summing the local SHC over the site index i : $\sigma_{\alpha\beta}^{S_\gamma} = \sum_i \sigma_{\alpha\gamma,i}^{S_\beta}$. We define the NC spin current as the local spin current whose spin polarization varies depending on atomic site i .

A unique direction of the spin polarization for the global spin current in the SHE is set by a mirror plane containing both an external electric field and electron's propagation path. This explains why an external electric field, electron's propagation, and the spin polarization are orthogonal to each other in cubic crystals. In Mn_3X , the mirror plane \mathcal{M}_{yz} [indicated by a green line in Fig. 2(a)] allows only for S_x polarization of the global spin Hall current flowing along z when an external electric field is applied along y . Because \mathcal{M}_{yz} transforms $Q_{zx} \rightarrow Q_{zx}$, $Q_{zy} \rightarrow -Q_{zy}$, and $Q_{zz} \rightarrow -Q_{zz}$ while \mathcal{E}_y remains invariant, $\sigma_{zy}^{S_y}$ and $\sigma_{zy}^{S_z}$ are not allowed.

In Mn_3X , however, not all sublattice atoms are located on top of \mathcal{M}_{yz} [Fig. 2(a)], which implies that the local spin Hall current can generally have NC polarization depending on the sublattice. Let us consider again a situation where an external electric field is applied along y and the spin Hall current is flowing along z , and analyze the structure of the

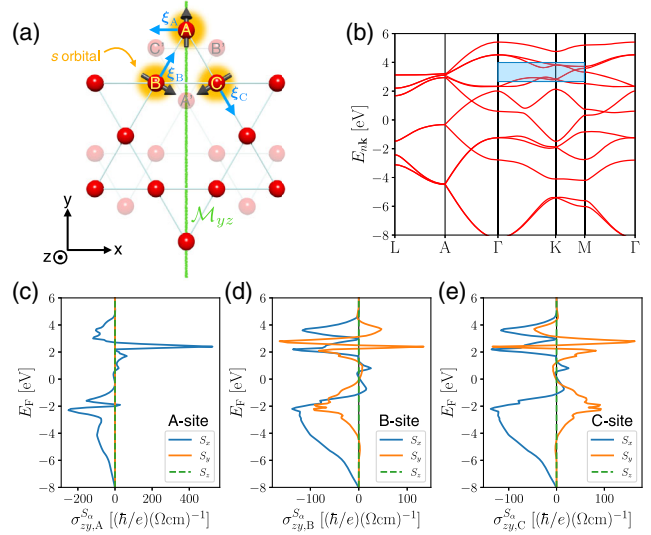


FIG. 2. (a) The structure of Mn_3X ($X = \text{Sn}, \text{Ge}$). Only Mn atom sites are shown as red spheres. There are 6 Mn atoms in a unit cell, and Mn atoms A, B, C in one layer are related to Mn atoms A' , B' , C' in another layer by the inversion symmetry. On each site, the magnetic moment of localized d electrons is indicated by black arrows, and conduction s electrons are depicted by orange clouds around the atoms. A mirror plane \mathcal{M}_{yz} is indicated by a green line. The chiral directions [Eq. (4)] are represented by blue arrows. (b) Electronic band structure according to the TB model of MnX_3 compounds. Shown are the local SHCs on (c) A site, (d) B site, and (e) C site, respectively.

local SHC tensor, $\sigma_{zy,i}^{S_\beta}$. On site A, only S_x polarization is allowed because the site index A is invariant with respect to \mathcal{M}_{yz} . However, on sites B and C, the spin current can have S_y polarization, which is a nontrivial direction, as well as S_x polarization. In general, there is no symmetry element that enforces them to vanish. Because site indices B and C are interchanged by \mathcal{M}_{yz} , these components are related by $\sigma_{zy,B}^{S_y} = -\sigma_{zy,C}^{S_y}$ and $\sigma_{zy,B}^{S_x} = \sigma_{zy,C}^{S_x}$. We remark that the NC spin current is “hidden” in this case: If the local SHCs are summed over all sites, only $\sigma_{zy}^{S_y}$ survives and $\sigma_{zy}^{S_x}$ vanishes. However, we remark that breaking of a mirror symmetry i.e., by a strain, thickness gradient, can induce occupation asymmetry of the hidden components, leading to an unconventional spin polarization of the global SHE [28]. Meanwhile, the components of the local SHC on sites A' , B' , C' are identical to those on sites A, B, C by the inversion symmetry. Detailed analysis of the symmetry can be found in the Supplemental Material [29].

In the following, we discuss only the time-reversal “even” component of the SHE. This means that the NC spin current we describe here arises even at the level of nonmagnetic crystals due to anisotropic crystal potential in combination with the spin-orbit coupling (SOC). This is different from the magnetic or time-reversal “odd” SHE [32–34], which arises from the magnetic texture.

We emphasize that, generally, the interplay of the local symmetry and magnetic order leads to a very rich structure of the NC spin current since the local SHC depends not only on the site index but also on the direction of local magnetic moments. We leave an investigation of such higher-order “magnetic” contributions to the NC spin current for future work.

For the demonstration of the emergence of NC spin current in Mn_3X , we adopt a tight-binding (TB) model [29]. As shown in Fig. 2(a), the unit cell contains six atoms on each Mn site. We assume that only s electrons are itinerant, and they interact with local magnetic moments of d electrons on site i (\mathbf{m}_i) via the sd exchange interaction. The Hamiltonian for the s electrons is written as

$$\begin{aligned} \mathcal{H}_{\text{el}} = & -t \sum_{\langle ij \rangle} \sum_{\alpha} c_{i\alpha}^{\dagger} c_{j\alpha} + J_{sd} \sum_i \sum_{\alpha\beta} c_{i\alpha}^{\dagger} (\boldsymbol{\sigma}_{\alpha\beta} \cdot \hat{\mathbf{m}}_i) c_{i\beta} \\ & + i\lambda \sum_{\langle ij \rangle} \sum_{\alpha\beta} c_{i\alpha}^{\dagger} \boldsymbol{\sigma}_{\alpha\beta} \cdot \hat{\mathbf{n}}_{ij} c_{j\beta}, \end{aligned} \quad (1)$$

where the first, second, and third terms describe intersite hopping, sd exchange coupling, and SOC. For site indices i, j , the notation $\langle \dots \rangle$ in the summation means that only nearest neighbors are taken into account. Here, $c_{i\alpha}$ ($c_{i\alpha}^{\dagger}$) is annihilation (creation) operator for the s orbital on site i with spin α and $\boldsymbol{\sigma}_{\alpha\beta}$ is a matrix element of the vector of Pauli matrices. The parameters are set as follows: $t = 1.0$ eV for the nearest neighbor hopping amplitude, $J_{sd} = 1.7$ eV for the sd exchange interaction with local moment $\hat{\mathbf{m}}_i$, $\lambda = 0.2$ eV for the strength of the SOC. Meanwhile, $\hat{\mathbf{n}}_{ij}$ is a unit vector orthogonal to both the hopping direction and the local crystal field. We set the direction of the magnetic moments by $\hat{\mathbf{m}}_A = \hat{\mathbf{y}}$, $\hat{\mathbf{m}}_B = (\sqrt{3}/2)\hat{\mathbf{x}} - (1/2)\hat{\mathbf{y}}$, and $\hat{\mathbf{m}}_C = -(\sqrt{3}/2)\hat{\mathbf{x}} - (1/2)\hat{\mathbf{y}}$.

The electronic band structure of the TB model is shown in Fig. 2(b), which agrees with the result from the previous study [35]. We evaluate the intrinsic local SHC from the TB model for the spin current flowing along z when an external electric field is applied along y . It is given by

$$\sigma_{zy,i}^{S_{\alpha}} = \frac{e}{\hbar} \sum_n \int \frac{d^3k}{(2\pi)^3} f_{nk} \Omega_{nk}^{S_{\alpha},zy,i}, \quad (2)$$

where

$$\Omega_{nk}^{S_{\alpha},zy,i} = 2\hbar^2 \sum_{m \neq n} \text{Im} \left[\frac{\langle u_{nk} | Q_{z\alpha,i} | u_{mk} \rangle \langle u_{mk} | v_y | u_{nk} \rangle}{(E_{nk} - E_{mk} + i\eta)^2} \right] \quad (3)$$

is the atom-projected spin Berry curvature. Here, $e > 0$ is the magnitude of the electron’s charge, \hbar is the reduced Planck constant, u_{nk} is periodic part of the Bloch state, and E_{nk} and f_{nk} are corresponding energy eigenvalue and Fermi-Dirac distribution, respectively. The calculated local SHCs on sites A, B, C are shown in Figs. 2(c)–2(e),

respectively, as a function of the Fermi energy E_F . As explained, the local SHC on site A has only S_x component and the other spin components are absent. On sites B and C, however, both S_x and S_y are present. This result is consistent with the symmetry analysis [29].

Considering a combined result of various components of the local conductivity tensor $\sigma_{zy,i}^{S_{\alpha}}$, we can define the “chiral” component of the SHC by

$$\sigma_{zy}^{S_{\text{ch}}} = \sum_{i,\alpha} \sigma_{zy,i}^{S_{\alpha}} \hat{\xi}_{\alpha,i}, \quad (4)$$

where $\hat{\xi}_A = -\hat{\mathbf{x}}$, $\hat{\xi}_B = (1/2)\hat{\mathbf{x}} + (\sqrt{3}/2)\hat{\mathbf{y}}$, $\hat{\xi}_C = (1/2)\hat{\mathbf{x}} - (\sqrt{3}/2)\hat{\mathbf{y}}$, determine the “chiral” directions on each site, which are indicated by blue arrows in Fig. 2(a). This is the component that enables coupling to the NC texture of magnetic moments in Mn_3X and inducing a NC spin torque, which goes beyond the uniform and staggered torques conventionally discussed in the context of ferromagnetic or Néel order switching.

Our calculation of the chiral SHC is shown in Fig. 3(a), which is compared with a uniform (S_x) component. We observe that while the uniform component has large values over a wide range of energy, the chiral component tends to exhibit a more spiky behavior. This is because it requires a “chiral” mixing of the spin character that can be achieved at specific \mathbf{k} points in the electronic structure. However, it is remarkable that the chiral component can be as large as the uniform component, especially near $E_F \approx -2$ eV and $E_F \approx +3$ eV [highlighted by a blue box in Fig. 2(b)], where various bands cross each other. To visualize the influence of band crossings, in Fig. 3(b), we plot the “chiral” spin Berry curvature near $E \approx +3$ eV along $\Gamma - K - M$, which is strongly pronounced near the band crossings.

In a Mn_3X film grown along [0001] direction (perpendicular to the Kagome plane), the chiral component of the NC spin current induced by an external electric field leads to a spin accumulation at both surfaces, which exerts a torque on local moments [29]. This is analogous to the self-induced torque driven by an intrinsic spin current from a ferromagnet in heterostructures with broken mirror

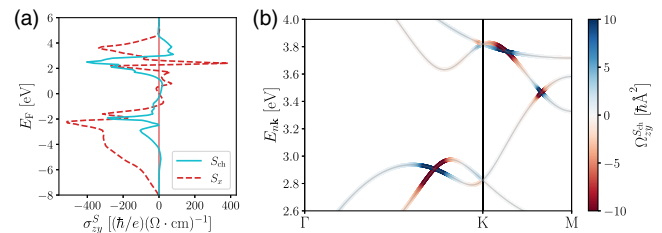


FIG. 3. (a) Comparison of the SHCs for the chiral component S_{ch} (cyan solid line) and a uniform component S_x (red dashed line) as a function of the Fermi energy. (b) “Chiral” spin Berry curvatures near the band crossings, which is indicated by color on top of the band structure.

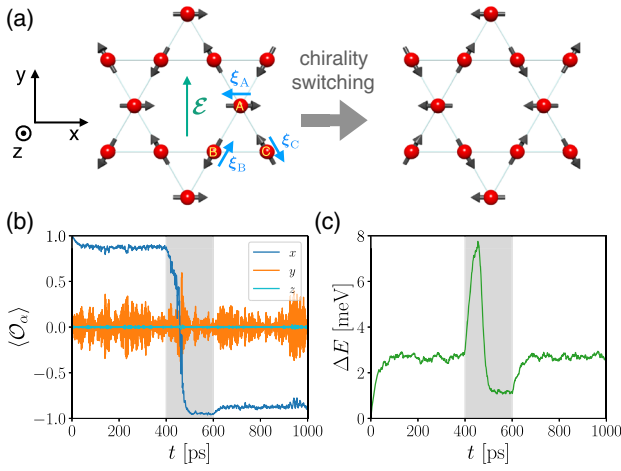


FIG. 4. (a) Chirality switching induced by the NC spin current, where black arrows represent local moments of Mn atoms in Mn_3X . An external electric field \mathcal{E} is indicated by a green arrow. Time evolution of (b) the average octupole moments and (c) energy per unit cell obtained from atomistic spin dynamics simulation. The chiral self-induced torque is applied during $t = 400\text{--}600$ ps.

symmetry [36,37]. While the self-induced torque cancels to zero for a freestanding film, interaction of the Mn_3X film and the substrate will cause an asymmetry between the top and bottom surfaces, leading to finite self-induced torque in a “chiral” manner. We propose an idea that the self-induced torque caused by the NC spin current can be used to switch the chiral magnetic texture of Mn_3X as illustrated in Fig. 4(a).

In order to demonstrate the switching of the chiral spin texture, we consider a classical spin model and perform the atomistic spin dynamics simulations [29,30]. For simplicity, we consider a single layer Kagome plane with three spins in the unit cell. The Hamiltonian for the spin system is given by

$$\mathcal{H}_{\text{mag}} = J \sum_{\langle ij \rangle} \hat{\mathbf{m}}_i \cdot \hat{\mathbf{m}}_j - \frac{K}{2} \sum_i (\hat{\mathbf{K}}_i \cdot \hat{\mathbf{m}}_i)^2 + D \sum_{\langle ij \rangle} \hat{\mathbf{n}}_{ij} \cdot (\hat{\mathbf{m}}_i \times \hat{\mathbf{m}}_j), \quad (5)$$

where $\hat{\mathbf{m}}_i$ is the direction of the magnetic moment of the d electrons at site i , $J > 0$ is the strength of the exchange interaction (antiferromagnetic), $K > 0$ is the strength of the in-plane anisotropy whose direction depends on the sublattice such that $\hat{\mathbf{K}}_A = \hat{\mathbf{x}}$, $\hat{\mathbf{K}}_B = -(1/2)\hat{\mathbf{x}} - (\sqrt{3}/2)\hat{\mathbf{y}}$, $\hat{\mathbf{K}}_C = -(1/2)\hat{\mathbf{x}} + (\sqrt{3}/2)\hat{\mathbf{y}}$, and D is the strength of the Dzyaloshinskii-Moriya interaction. The definition of $\hat{\mathbf{n}}_{ij}$ is identical to that in Eq. (1). Based on Eq. (5), we solve a stochastic Landau-Lifshitz-Gilbert equation by applying a chiral torque of the form $\boldsymbol{\tau}_i^{\text{chiral}} = (\tau_0 |\gamma| / \mu_B) \hat{\mathbf{m}}_i \times (\hat{\boldsymbol{\xi}}_i \times \hat{\mathbf{m}}_i)$, where τ_0 is the magnitude of the torque, γ is the

gyromagnetic ratio, μ_B is the Bohr magneton, and $\hat{\boldsymbol{\xi}}_i$'s are the chiral directions defined in Eq. (4) and indicated by blue arrows in Fig. 4(a). This torque enables switching of the chiral magnetic texture via a soft mode that coherently rotates the magnetic moments in the Kagome plane [38,39]. For magnetic interaction parameters, we choose $J = 10$, $K = 0.1$, $D = 0.7$ in units of meV. The Gilbert damping constant and the temperature are set $\alpha = 0.001$ and $T = 10$ K, respectively. The magnitude of the local moment on each site is assumed to be $m_0 = 3\mu_B$.

For the analysis, we define an order parameter of Mn_3X by

$$\mathcal{O} = \frac{1}{3} (\hat{\mathbf{m}}_A + R\hat{\mathbf{m}}_B + R^2\hat{\mathbf{m}}_C), \quad (6)$$

where R is an anticlockwise rotation by $2\pi/3$ around the z axis [40]. For the ground state configurations shown in Fig. 4(a), for example, $\mathcal{O} = \hat{\mathbf{m}}_A$ when $T = 0$. We remark that \mathcal{O} is often referred to as the octupole magnetic moment in the literature [18,22,41,42]. In Fig. 4(b), we show the evolution of \mathcal{O} averaged over the 10×10 supercell. The torque is applied from $t = 400$ ps until $t = 600$ ps (marked by gray color shade). A plot for \mathcal{O}_x (blue line) clearly shows that the chiral magnetic texture is switched by the torque within ~ 100 ps interval. Meanwhile we observe fluctuation of the other components. Overall, \mathcal{O}_y exhibits stronger fluctuation than \mathcal{O}_z , which is attributed to the in-plane anisotropy of the system. It is interesting to notice that the fluctuation becomes enhanced during the switching ($t \approx 450$ ps). Evaluation of the energy in each time step by Eq. (5) is shown in Fig. 4(c). It reveals the activation energy required for the switching is $\Delta E \approx 8$ meV per unit cell. While the overall background fluctuation of $\Delta E \approx 2.5$ meV is due to thermal effect, the energy fluctuations becomes suppressed when the torque is still applied after the switching at $t \approx 500$ ps.

As we have demonstrated, the torque exerted by the NC spin current can result in the field-free switching of the chiral magnetic texture in Mn_3X as the degeneracy of the two spin configurations in Fig. 4(a) is lifted. In contrast, the collinear spin current does not lift the degeneracy, which results in continuous precession if there is no external magnetic field [23]. Thus, for the collinear spin current, switching the magnetic texture of NC AFMs requires an external magnetic field to break the symmetry [22]. Therefore, the NC spin current is *essential* to achieve a deterministic switching of NC magnetic textures in AFMs without an external magnetic field. Moreover, the NC spin current is expected to be more efficient than the collinear spin current for switching because the geometry of the spin injection on each sublattice is optimal.

In conclusion, we propose a concept of the NC spin current that can be excited by the SHE in crystals with low local symmetry such as Mn_3X . As it arises from the

sublattice-dependent crystal potential, we expect that the NC spin current can be found in many other materials, where the crystal potentially is locally asymmetric, e.g., altermagnets [43]. A major consequence of the NC spin current results from its coupling with the chiral magnetic texture in NC AFMs. For example, in a thin film of Mn_3X grown on a substrate, the NC spin current may result in a self-induced torque at the interface and switch the chirality of the magnetic texture. This opens a novel route toward electric control of NC AFMs that can be applied, for example, for a memory device that stores information in the magnetic configuration in a NC AFM that can be controlled by the NC spin current. Moreover, the NC spin current can be used to excite magnon modes in AFMs that do not couple to collinear spin currents [38]. As such, our finding is an important manifestation of a sublattice-dependent electronic excitations and its coupling to a magnetic texture, which is “hidden” in the description of global spin current, and it is expected to play a crucial role in understanding complex nature of spin excitations in chiral magnets.

We thank Hiroshi Katsumoto, Adithya Rajan, Arnab Bose, Tom G. Saunderson, and Mathias Kläui for fruitful discussions. We gratefully acknowledge the Jülich Supercomputing Centre for providing computational resources under Project No. jiff40. This work was funded by the Deutsche Forschungsgemeinschaft (DFG, German Research Foundation)—TRR 173/2-268565370 Spin + X (Projects No. A11 and No. B12), TRR 288—422213477 (Projects No. A09 and No. B06), CRC 1238—277146847 (Project C06), SPP 2137 “Skyrmionics” (Grand No. BL 444/16-2), and the Sino-German research project DISTOMAT (MO 1731/10-1). O. G. acknowledges EU FET Open RIA Grant No. 766566.

*Corresponding author.

d.go@fz-juelich.de

†Corresponding author.

y.mokrousov@fz-juelich.de

- [1] T. Jungwirth, X. Marti, P. Wadley, and J. Wunderlich, Antiferromagnetic spintronics, *Nat. Nanotechnol.* **11**, 231 (2016).
- [2] V. Baltz, A. Manchon, M. Tsoi, T. Moriyama, T. Ono, and Y. Tserkovnyak, Antiferromagnetic spintronics, *Rev. Mod. Phys.* **90**, 015005 (2018).
- [3] F. Keffer and C. Kittel, Theory of antiferromagnetic resonance, *Phys. Rev.* **85**, 329 (1952).
- [4] P. Ross, M. Schreier, J. Lotze, H. Huebl, R. Gross, and S. T. B. Goennenwein, Antiferromagnetic resonance detected by direct current voltages in MnF_2/Pt bilayers, *J. Appl. Phys.* **118**, 233907 (2015).
- [5] O. Gomonay, V. Baltz, A. Brataas, and Y. Tserkovnyak, Antiferromagnetic spin textures and dynamics, *Nat. Phys.* **14**, 213 (2018).
- [6] J. Železný, H. Gao, K. Výborný, J. Zemen, J. Mašek, A. Manchon, J. Wunderlich, J. Sinova, and T. Jungwirth, Relativistic Néel-Order Fields Induced by Electrical Current in Antiferromagnets, *Phys. Rev. Lett.* **113**, 157201 (2014).
- [7] P. Wadley *et al.*, Electrical switching of an antiferromagnet, *Science* **351**, 587 (2016).
- [8] J. Železný, H. Gao, A. Manchon, F. Freimuth, Y. Mokrousov, J. Zemen, J. Mašek, J. Sinova, and T. Jungwirth, Spin-orbit torques in locally and globally non-centrosymmetric crystals: Antiferromagnets and ferromagnets, *Phys. Rev. B* **95**, 014403 (2017).
- [9] S. Y. Bodnar, L. Šmejkal, I. Turek, T. Jungwirth, O. Gomonay, J. Sinova, A. A. Sapozhnik, H.-J. Elmers, M. Kläui, and M. Jourdan, Writing and reading antiferromagnetic Mn_2Au by Néel spin-orbit torques and large anisotropic magnetoresistance, *Nat. Commun.* **9**, 348 (2018).
- [10] M. Meinert, D. Graulich, and T. Matalla-Wagner, Electrical Switching of Antiferromagnetic Mn_2Au and the Role of Thermal Activation, *Phys. Rev. Applied* **9**, 064040 (2018).
- [11] X. F. Zhou, J. Zhang, F. Li, X. Z. Chen, G. Y. Shi, Y. Z. Tan, Y. D. Gu, M. S. Saleem, H. Q. Wu, F. Pan, and C. Song, Strong Orientation-Dependent Spin-Orbit Torque in Thin Films of the Antiferromagnet Mn_2Au , *Phys. Rev. Applied* **9**, 054028 (2018).
- [12] H. Chen, Q. Niu, and A. H. MacDonald, Anomalous Hall Effect Arising from Noncollinear Antiferromagnetism, *Phys. Rev. Lett.* **112**, 017205 (2014).
- [13] J. Kbler and C. Felser, Non-collinear antiferromagnets and the anomalous Hall effect, *Europhys. Lett.* **108**, 67001 (2014).
- [14] S. Nakatsuji, N. Kiyohara, and T. Higo, Large anomalous Hall effect in a non-collinear antiferromagnet at room temperature, *Nature (London)* **527**, 212 (2015).
- [15] A. K. Nayak, J. E. Fischer, Y. Sun, B. Yan, J. Karel, A. C. Komarek, C. Shekhar, N. Kumar, W. Schnelle, J. Kbler, C. Felser, and S. S. P. Parkin, Large anomalous Hall effect driven by a nonvanishing Berry curvature in the noncollinear antiferromagnet Mn_3Ge , *Sci. Adv.* **2**, e1501870 (2016).
- [16] M. Ikhlas, T. Tomita, T. Koretsune, M.-T. Suzuki, D. Nishio-Hamane, R. Arita, Y. Otani, and S. Nakatsuji, Large anomalous Nernst effect at room temperature in a chiral antiferromagnet, *Nat. Phys.* **13**, 1085 (2017).
- [17] H. Reichlova, T. Janda, J. Godinho, A. Markou, D. Kriegner, R. Schlitz, J. Zelezny, Z. Soban, M. Bejarano, H. Schultheiss, P. Nemeč, T. Jungwirth, C. Felser, J. Wunderlich, and S. T. B. Goennenwein, Imaging and writing magnetic domains in the non-collinear antiferromagnet Mn_3Sn , *Nat. Commun.* **10**, 5459 (2019).
- [18] T. Higo, H. Man, D. B. Gopman, L. Wu, T. Koretsune, O. M. J. van 't Erve, Y. P. Kabanov, D. Rees, Y. Li, M.-T. Suzuki, S. Patankar, M. Ikhlas, C. L. Chien, R. Arita, R. D. Shull, J. Orenstein, and S. Nakatsuji, Large magneto-optical Kerr effect and imaging of magnetic octupole domains in an antiferromagnetic metal, *Nat. Photonics* **12**, 73 (2018).
- [19] K. Kuroda, T. Tomita, M.-T. Suzuki, C. Bareille, A. A. Nugroho, P. Goswami, M. Ochi, M. Ikhlas, M. Nakayama, S. Akebi, R. Noguchi, R. Ishii, N. Inami, K. Ono, H. Kumigashira, A. Varykhalov, T. Muro, T. Koretsune, R. Arita, S. Shin, T. Kondo, and S. Nakatsuji, Evidence for

- magnetic Weyl fermions in a correlated metal, *Nat. Mater.* **16**, 1090 (2017).
- [20] H. Nielsen and M. Ninomiya, The Adler-Bell-Jackiw anomaly and Weyl fermions in a crystal, *Phys. Lett.* **130B**, 389 (1983).
- [21] N. P. Armitage, E. J. Mele, and A. Vishwanath, Weyl and Dirac semimetals in three-dimensional solids, *Rev. Mod. Phys.* **90**, 015001 (2018).
- [22] H. Tsai, T. Higo, K. Kondou, T. Nomoto, A. Sakai, A. Kobayashi, T. Nakano, K. Yakushiji, R. Arita, S. Miwa, Y. Otani, and S. Nakatsuji, Electrical manipulation of a topological antiferromagnetic state, *Nature (London)* **580**, 608 (2020).
- [23] Y. Takeuchi, Y. Yamane, J.-Y. Yoon, R. Itoh, B. Jinnai, S. Kanai, J. Ieda, S. Fukami, and H. Ohno, Chiral-spin rotation of non-collinear antiferromagnet by spin-orbit torque, *Nat. Mater.* **20**, 1364 (2021).
- [24] O. V. Gomonay and V. M. Loktev, Using generalized Landau-Lifshitz equations to describe the dynamics of multi-sublattice antiferromagnets induced by spin-polarized current, *Low Temp. Phys.* **41**, 698 (2015).
- [25] S. Dasgupta and O. A. Tretiakov, Tuning the Hall response of a non-collinear antiferromagnet with spin-transfer torques, [arXiv:2202.06882](https://arxiv.org/abs/2202.06882).
- [26] F. Freimuth, S. Blügel, and Y. Mokrousov, Anisotropic Spin Hall Effect from First Principles, *Phys. Rev. Lett.* **105**, 246602 (2010).
- [27] T. c. v. Rauch, F. Töpler, and I. Mertig, Local spin Hall conductivity, *Phys. Rev. B* **101**, 064206 (2020).
- [28] A. Roy, M. H. D. Guimares, and J. Sawiska, Unconventional spin Hall effects in nonmagnetic solids, *Phys. Rev. Mater.* **6**, 045004 (2022).
- [29] See Supplemental Material at <http://link.aps.org/supplemental/10.1103/PhysRevLett.129.097204> for the symmetry analysis of site-dependent spin Hall currents, detailed information on the tight-binding model, simulation of self-induced torque in a thin film, and details on the spin dynamics simulation, which contains Refs. [30,31].
- [30] G. P. Müller, M. Hoffmann, C. Dißelkamp, D. Schürhoff, S. Mavros, M. Sallermann, N. S. Kiselev, H. Jónsson, and S. Blügel, Spirit: Multifunctional framework for atomistic spin simulations, *Phys. Rev. B* **99**, 224414 (2019).
- [31] M. I. Aroyo, J. M. Perez-Mato, C. Capillas, E. Kroumova, S. Ivantchev, G. Madariaga, A. Kirov, and H. Wondratschek, Bilbao crystallographic server: I. Databases and crystallographic computing programs, *Z. Kristallogr.-Cryst. Mater.* **221**, 15 (2006).
- [32] J. Železný, Y. Zhang, C. Felser, and B. Yan, Spin-Polarized Current in Noncollinear Antiferromagnets, *Phys. Rev. Lett.* **119**, 187204 (2017).
- [33] M. Kimata, H. Chen, K. Kondou, S. Sugimoto, P. K. Muduli, M. Ikhlas, Y. Omori, T. Tomita, A. H. MacDonald, S. Nakatsuji, and Y. Otani, Magnetic and magnetic inverse spin Hall effects in a non-collinear antiferromagnet, *Nature (London)* **565**, 627 (2019).
- [34] A. Mook, R. R. Neumann, A. Johansson, J. Henk, and I. Mertig, Origin of the magnetic spin Hall effect: Spin current vorticity in the Fermi sea, *Phys. Rev. Research* **2**, 023065 (2020).
- [35] N. Ito and K. Nomura, Anomalous Hall effect and spontaneous orbital magnetization in antiferromagnetic Weyl metal, *J. Phys. Soc. Jpn.* **86**, 063703 (2017).
- [36] W. Wang, T. Wang, V. P. Amin, Y. Wang, A. Radhakrishnan, A. Davidson, S. R. Allen, T. J. Silva, H. Ohldag, D. Balzar, B. L. Zink, P. M. Haney, J. Q. Xiao, D. G. Cahill, V. O. Lorenz, and X. Fan, Anomalous spin-orbit torques in magnetic single-layer films, *Nat. Nanotechnol.* **14**, 819 (2019).
- [37] D. Cspedes-Berrocal, H. Damas, S. Petit-Watlot, D. Maccariello, P. Tang, A. Arriola-Crdova, P. Vallobra, Y. Xu, J.-L. Bello, E. Martin, S. Migot, J. Ghanbaja, S. Zhang, M. Hehn, S. Mangin, C. Panagopoulos, V. Cros, A. Fert, and J.-C. Rojas-Sánchez, Current-induced spin torques on single GdFeCo magnetic layers, *Adv. Mater.* **33**, 2007047 (2021).
- [38] S. Dasgupta and O. Tchernyshyov, Theory of spin waves in a hexagonal antiferromagnet, *Phys. Rev. B* **102**, 144417 (2020).
- [39] Y. Chen, J. Gaudet, S. Dasgupta, G. G. Marcus, J. Lin, T. Chen, T. Tomita, M. Ikhlas, Y. Zhao, W. C. Chen, M. B. Stone, O. Tchernyshyov, S. Nakatsuji, and C. Broholm, Antichiral spin order, its soft modes, and their hybridization with phonons in the topological semimetal Mn_3Ge , *Phys. Rev. B* **102**, 054403 (2020).
- [40] E. V. Gomonaj and V. A. L'vov, Phenomenologic study of phase transitions in noncollinear antiferromagnets of metallic perovskite type, *Phase Transitions* **38**, 15 (1992).
- [41] M.-T. Suzuki, T. Koretsune, M. Ochi, and R. Arita, Cluster multipole theory for anomalous Hall effect in antiferromagnets, *Phys. Rev. B* **95**, 094406 (2017).
- [42] T. Nomoto and R. Arita, Cluster multipole dynamics in noncollinear antiferromagnets, *Phys. Rev. Research* **2**, 012045(R) (2020).
- [43] L. Šmejkal, J. Sinova, and T. Jungwirth, Altermagnetism: Spin-momentum locked phase protected by non-relativistic symmetries, [arXiv:2105.05820](https://arxiv.org/abs/2105.05820).